Lasing in localized mode at optimized photonic amorphous structure

Kwang-Yong Jeong, Yong-Hee Lee, Hui Cao, and Jin-Kyu Yang

Citation: Appl. Phys. Lett. **101**, 091101 (2012); doi: 10.1063/1.4748109
View online: http://dx.doi.org/10.1063/1.4748109
View Table of Contents: http://apl.aip.org/resource/1/APPLAB/v101/i9
Published by the American Institute of Physics.

Lasing in localized mode at optimized photonic amorphous structure

Kwang-Yong Jeong,[1] Yong-Hee Lee,[1] Hui Cao,[2] and Jin-Kyu Yang[3,4,a)]
[1]*Department of Physics, KAIST, Daejeon 305-701, South Korea*
[2]*Department of Applied Physics, Yale University, New Haven, Connecticut 06511, USA*
[3]*Department of Optical Engineering, Kongju National University, Kongju 314-701, South Korea*
[4]*Optics and Photonics Elite Research Academy (OPERA), Inha University, Incheon 402-751, South Korea*

(Received 23 July 2012; accepted 13 August 2012; published online 27 August 2012)

We demonstrated lasing in localized modes of an optimized photonic amorphous structure with short-range order. The InGaAsP multiple quantum wells embedded in a free-standing InGaAsP slab were employed as an active medium by optical pumping at room temperature. The high index contrast between air and InGaAsP, combined with uniformity of local topology and short-range order, enables strong confinement of light via multiple scattering. We confirmed the characteristic of lasing modes in the complex geometry with numerical simulations based on the real images of fabricated samples. © *2012 American Institute of Physics*. [http://dx.doi.org/10.1063/1.4748109]

Photonic crystals (PCs) with periodic arrangement of dielectric media have attracted much research interest because of their fascinating optical properties, e.g., the photonic band-gap (PBG) effect to prohibit light propagation within certain frequency range.[1] The rapid advances in PCs led to the realization of various functional devices, such as photonic waveguides, lasers, optical filters, and photodetecters.[2–5] Similarly, photonic amorphous structures (PAS) have short range order which improves light confinement at a certain frequency due to enhanced scattering. While the PBG of a PC is formed by the interference effect of periodic arrangement of media, the PAS have the PBG formed by coupling of Mie resonances of individual scatterers with high refractive index. The PBG of a PAS is always isotropic due to the structural isotropy.

Recently, we studied the evolution of the PBG from PCs to PAS and found that even when the PBG disappears, there is still strong confinement of light near the frequency of the original PBG.[6] Especially, despite the lack of a PBG, biomimetic PAS could improve the confinement of light and enhance lasing action.[7,8] This implies that the structural factor is an important factor to enhance multiple scattering. Meanwhile, the geometry of scatterer is another important factor, because it can be optimized for maximal scattering cross section. Typically, the Mie scattering of a dielectric cylinder in air is more significant than that of the air cylinder in the dielectric medium. Therefore, in order to improve light confinement in a random structure consisting of dielectric cylinders, one should fix the size of cylinders and utilize the effect of proximity resonance.[9,10] In contrast, in a random structure with connected dielectric material, a uniform topology of the dielectric part is shown to be more efficient in confining light.[11,12] These studies show that the local structural uniformity of dielectric area, let it be the dielectric cylinders in an isolated system or dielectric channels in a connected system, is crucial to the construction of PBG.[13] In this paper, we propose an optimized PAS with constant separation of air holes in a high-index semiconductor for a strong light localization and demonstrate lasing action at room temperature by optical pumping.

Two-dimensional (2-D) amorphous patterns were created by a jammed packing method with poly-disperse air holes in the dielectric medium by computer simulations in order to preserve short-range order.[6] Then, the radii of all holes were reduced by the same amount to make the constant separation between the neighboring holes as shown in Fig. 1(a). The holes are considered to be air and embedded in a dielectric material of refractive index n. The filling fraction of air is set at 50%. Although the air holes are not uniform in size, the dielectric gap between the air holes has similar width. Thus this structure, labelled as constant-gap, has local uniformity in the dielectric topology. For comparison, we consider another structure with local uniformity in the air part, namely the 2D amorphous pattern with the constant size of air holes at the same center positions as shown in Fig. 1(b), and it is labelled constant-hole. First, we checked the statistical distribution of the dielectric spacing between the nearest neighbor holes in both structures as shown in Fig. 1(c). In constant-gap PAS, the peak value of probability distribution is about 50% with <3 nm full-width half maximum (FWHM) at 110-nm separation. However, in the constant-hole PAS, the peak value is about 3.5% with <3 nm FWHM at 105-nm separation. For a quantitative understanding of the local uniformity of the dielectric topology, an effective refractive index, n_{eff}, and its standard deviation, $\sigma(n)/n_{eff}$, were calculated as a function of sampling area. The sampling area is a circular disk of radius R_S centered at the centroid of a triangle made by the center positions of the three closest air holes as shown in the inset of Fig. 1(d).[11] The refractive index averaged within the sampling area displays nearly identical dependence on a_{ave}, because the center positions of air holes are identical in the constant-gap and constant-hole PAS. The variance $\sigma(n)/n_{eff}$, however, is significant different, as shown in Fig. 1(d). When the sampling area is small, it contains only the dielectric material not the air, so the standard deviation is zero. However, as the sampling area increases, the standard deviation increases because air holes are partially included in

a)Electronic mail: jinkyuyang@kongju.ac.kr.

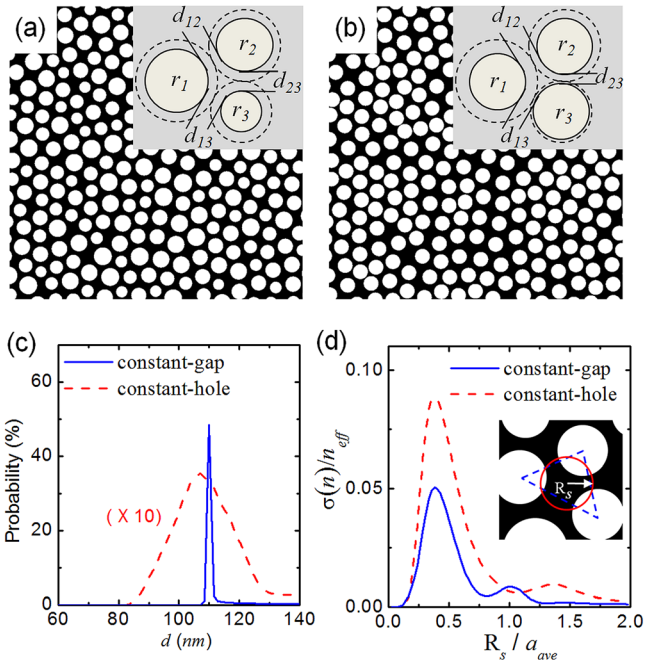

FIG. 1. (a),(b) Computer generated (a) local-uniform PAS with the constant separation of air holes and (b) mono-disperse PAS with air holes. (c) Statistical distribution of the dielectric spacing between the nearest neighbor holes. (d) The standard deviation of effective dielectric constant, n_{eff} as a function of a sampling size.

the sampling area. When the sampling area becomes much larger than the hole diameter, the standard deviation is reduced because the sampling area contains many air holes. The standard deviation $\sigma(n)/n_{eff}$ in the constant-gap PAS is smaller than that in the constant-hole structure, implying the former has higher degree of local uniformity.

In order to understand how local structural uniformity of dielectric medium affects optical properties, three-dimensional (3-D) density of optical states (DOS) transverse-electric (TE)-like polarized light was calculated using order-N method.[6] Here, free-standing InGaAsP slab structures with air holes were considered. The thickness of InGaAsP slab, the average distance between nearest air holes, a_{ave}, and the refractive index of InGaAsP at $\lambda \sim 1.5\mu$m are 270 nm, 485 nm, and 3.2, respectively. As seen in Fig. 2(a), the constant-gap PAS displays a pseudo bandgap behaviour inside the original PBG of a PC with a triangular lattice of air holes, even though the gap depth and width are significantly reduced. In contrast, the constant-hole PAS does not exhibit any dip in DOS. This difference is attributed to the fact that the dielectric topology in the constant-gap PAS is more uniform than that in the constant-hole PAS. Hence, the partial depletion of photonic DOS in the constant-gap leads to an improvement of light confinement and the formation of high quality factor (Q-factor) modes. For a further understanding of the local structural effect on the light confinement, we calculated Q-factors of localized modes by 3D-FDTD simulation with the boundary condition of a perfect matched layer. Figure 2(b) shows the Q factor distribution as a function of the normalized frequency. The maximal Q-factor mode is found at the frequency of minimal DOS. More specifically, the maximum Q value in the constant-gap PAS is about 2100 ($a/\lambda = 0.300$), while it is less than 980 in the constant-hole PAS.

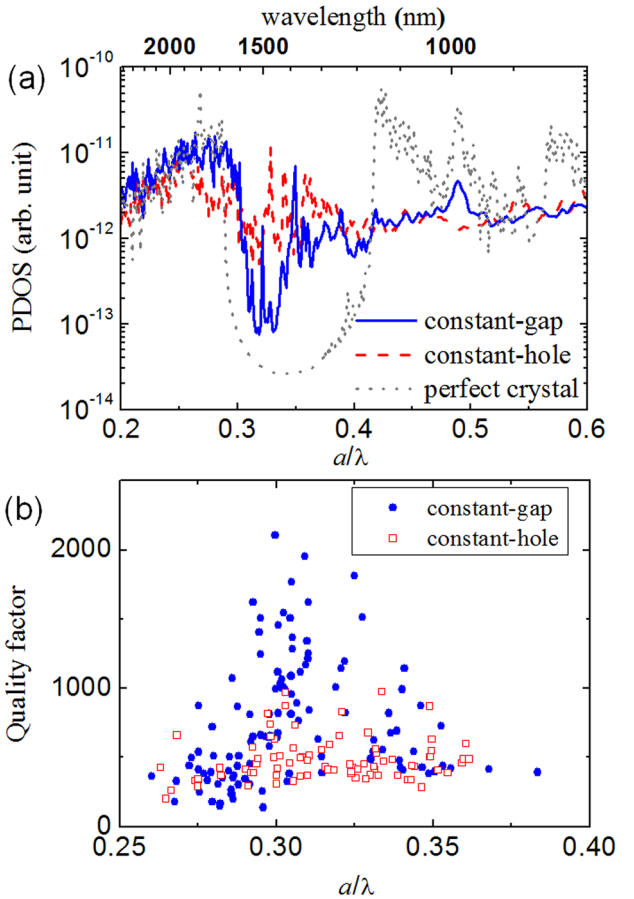

FIG. 2. (a) Calculated density of optical states for constant-gap PAS (blue solid line) and constant-hole PAS (red dashed line) in InGaAsP slab. The gray dotted line represents the DOS for a photonic crystal with a triangular lattice of air holes. (b) The quality factor of resonant modes in the constant-gap PAS (solid circle) and the constant-hole PAS (open square) as a function of the normalized frequency a/λ, where a is the average spacing of air holes and the λ is the wavelength in air.

Next we used the stronger confinement of light in the constant-gap PAS for lasing. We fabricated 2D constant-gap PAS structures in a free-standing 270-nm-thick InGaAsP slab. Seven InGaAsP quantum wells are embedded in the slab, and their photoluminescence (PL) peak is at 1.55 μm.[3,5] First, the computer-generated patterns are written onto a 200-nm-thick polymethyl methacrylate (PMMA) layer on top of InGaAsP slab by standard electron-beam lithography. After hardening of the patterned PMMA layer by Ar ion bombardment, the pattern is transferred into the InGaAsP slab and the InP sacrificial layer underneath by the chemically assisted ion beam etching. Finally, a free-standing InGaAsP slab structure is formed by wet etching of the InP sacrificial layer in a dilute HCl solution. Figure 3(a) shows the top-view scanning electron microscope (SEM) image of a fabricated PAS with constant dielectric gap. The averaged distance between nearest neighbor holes is about 485 nm, and the average diameter of air holes is about 320 nm in the center. Because of the proximity effect of electron beam lithography, the air holes near the boundary are smaller. The diameter of the patterns was only about 11 μm. In the lasing experiments, the samples were optically pumped by a pulsed diode laser (pulse width $\sim$10 ns, center wavelength $\sim$980 nm, and pulse repetition rate $\sim$1 MHz) at room temperature. A 50$\times$ objective lens (numerical aperture = 0.85) focused the pump

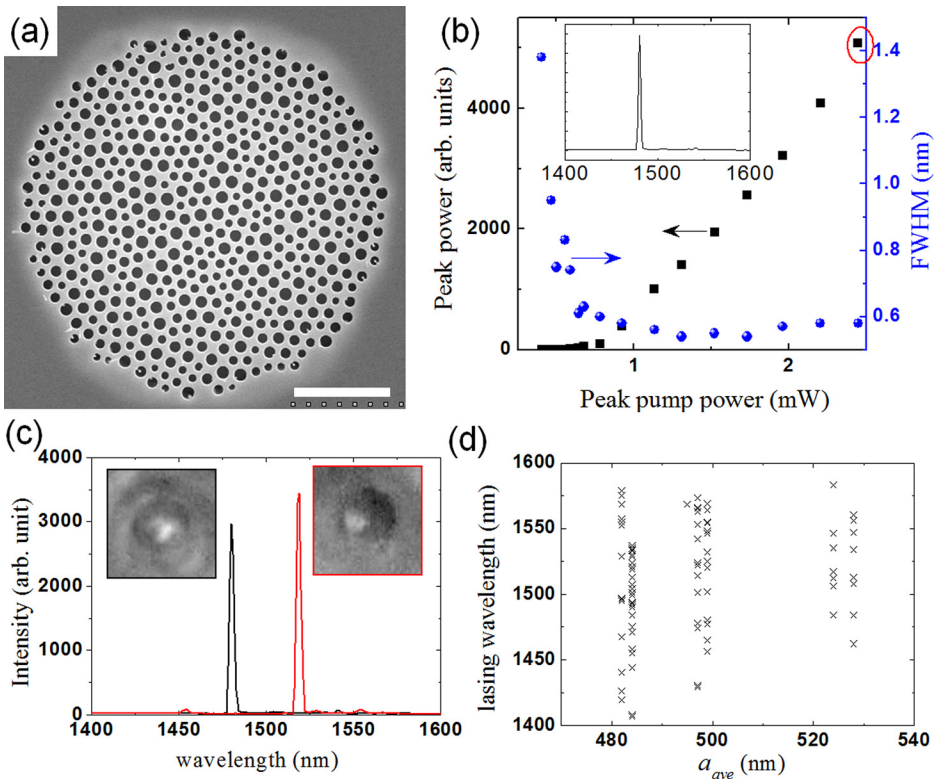

FIG. 3. (a) Top-view SEM image of a fabricated constant-gap PAS in an InGaAsP membrane. The scale bar is 3 μm. (b) Intensity and spectral width of the emission peak at $\lambda = 1480$ nm as a function of the peak pump power. The inset is the measured spectrum at an incident pump power of $P = 2.45$ mW. (c) The lasing spectra taken two different locations of the pump spot. The left (right) inset is the near-field image of the pump spot when lasing at $\lambda = 1480$ nm ($\lambda = 1520$ nm). (d) Measured wavelengths of lasing peaks for PAS with different a_{ave}.

light to a pattern at normal incidence. The diameter of pump spot on the sample surface was about 3 μm. The emission from the sample was collected by the same objective lens. The emission spectrum was measured by a monochromator with an InGaAs detector. The spatial distribution of emission intensity across the sample surface was projected onto an infra-red charged-carrier-device (CCD) camera, simultaneously.

Figure 3(b) shows the typical lasing behaviour of a mode in the constant-gap PAS. The inset is the lasing spectrum above threshold (peak power $P = 2.45$ mW). The intensity and linewidth of the emission peak at $\lambda \sim 1480$ nm exhibit a threshold dependence on the peak pump power. The lasing threshold is estimated to be about 700 μW, which is a little higher than a typical PC defect laser.[14] The linewidth at high pump power is limited by the resolution of spectrometer. As the pump beam spot was moved around the patterned area, new lasing peaks replaced the existing one, but their wavelengths are distinct. Figure 3(c) shows two emission spectra, taken at different pump positions. The insets were the near-field images of lasing above threshold with illumination light. The dark circular region in each image is the patterned area. When we pumped the center of the pattern, the dominant lasing mode is at $\lambda = 1480$ nm. However, when we pumped the left of the pattern, the main lasing mode is at $\lambda = 1520$ nm. Such phenomena indicate that there are many resonant modes in the pattern, and they are localized at different positions. Many of them can be brought to lasing when overlapped with the pumping spot.

We repeated the lasing experiment on multiple PAS patterns with different values of a_{ave}. These patterns were created from the jammed packing algorithm different initial seeds, so their structural factor and local uniformity were nearly identical. Figure 3(d) plots the lasing wavelengths for samples of different a_{ave}, which ranges from 482 nm to 528 nm. The lasing peaks were widely distributed in the gain spectrum of the InGaAsP QWs. The wavelength range of lasing peaks, e.g., for $a_{ave} = 482$ nm, is well matched with the pseudo-bandgap region, 1410 nm –1580 nm in Fig. 2(a). As a_{ave} increases, the lasing peaks move to longer wavelength, following the red shift of the pseudo PBG with a_{ave}.

To reveal the nature of the lasing modes, we performed 3D FDTD simulation of the real structures that were extracted from the digitized SEM images. Figure 4(a) shows the electric field intensity distribution of a resonant mode in the constant-gap PAS with $a_{ave} = 485$ nm. The calculated wavelength $\lambda = 1566$ nm, which is about 5% different from the lasing peak wavelength measured experimentally. This error might be caused by a slight mismatch of the thickness and/or the refractive index of InGaAsP slab. The numerical results illustrated that the lasing mode corresponds to a strongly localized resonance. Its electric field is concentrated in the dielectric region, thus beneficial to lasing due to large overlap with the gain material. The calculated Q factor was about 3300, similar to the experimental Q factor, ~2500, estimated at transparent point (~677 μW). The optical loss due to out-of-plane leakage of light is about ten times higher than the in-plane leakage. Therefore, Q factor was limited by the out-of-plane leakage owing to strong in-plane localization of light. We also calculated the time-averaged power flux (projected Poynting vector) in the direction normal to the slab surface in order to compare with the CCD-captured image of laser emission as shown in Fig. 4(b). The projected Poynting vector was probed in the plane of a distance $\sim\lambda$ from the surface of the slab and averaged within one period time. As shown in the inset of Fig. 4(b), the calculated power flux agrees with the spatial distribution of laser emission.

In summary, we proposed and demonstrated an optimized PAS that combines the local uniformity of dielectric

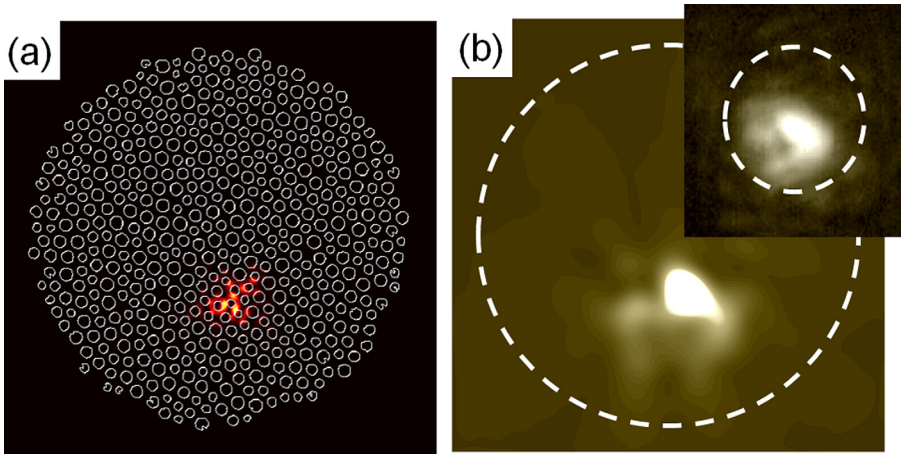

FIG. 4. Numerical simulation results based on the digitized SEM image of a fabricated constant-gap PAS with $a_{ave} = 485\,\text{nm}$. (a) Electric field intensity distribution of a resonant mode at $\lambda = 1566\,\text{nm}$. (b) Calculated time-averaged Poynting vector projected onto the vertical direction on a plane of distance $1.5\,\mu\text{m}$ from the top surface of the slab. The inset is the near-field image above threshold captured by the IR CCD camera. The dashed lines mark the boundary of the PAS.

topology with the short-range order. We realized lasing in the localized modes by optical pumping at room temperature and confirmed characteristic of lasing modes by numerical simulation of the real structures extracted from the SEM images. The modes were strongly localized in the dielectric region, and different modes are selected for lasing by shifting the position of pump light. By varying the structural parameters, we can tune the lasing frequency within the gain spectrum. The optimized PAS may be a good candidate for integrated nanophotonic circuits because of the pseudo PBG and robustness against structural disorder caused by fabrication error.

The authors thank Professor Corey S. O'Hern and Carl Schreck for computer generation of jammed packing of cylinders and Professor M. K. Seo for supporting parallel FDTD code. This work is supported by the Basic Science Research Program through the NRF funded by the Korean government (MEST) (2011-0015030), and KOSEF through OPERA (R11-2003-22).

[1]Y. Yablonovitch, Phys. Rev. Lett. **58**, 2059 (1987).
[2]M. Notomi, H. Suzuki, T. Tamamura, and K. Edagawa, Phys. Rev. Lett. **92**, 123906 (2004).
[3]H.-G. Park, S.-H. Kim, S.-H. Kwon, Y.-G. Ju, J.-K. Yang, J.-H. Baek, S.-B. Kim, and Y.-H. Lee, Science **305**, 1444 (2004).
[4]S. Noda, A. Chutinan, and M. Imada, Nature (London) **407**, 608 (2000).
[5]J.-K. Yang, M.-K. Seo, I.-K. Hwang, S.-B. Kim, and Y.-H. Lee, Appl. Phys. Lett. **93**, 211103 (2008).
[6]J.-K. Yang, C. Schreck, H. Noh, S. F. Liew, M. I. Guy, C. S. O'Hern, and H. Cao, Phys. Rev. A **82**, 053838 (2010).
[7]J.-K. Yang, H. Noh, S. F. Liew, M. J. Rooks, G. S. Solomon, and H. Cao, Phys. Rev. A **84**, 033820 (2011).
[8]H. Noh, J.-K. Yang, S. F. Liew, M. J. Rooks, G. S. Solomon, and H. Cao, Phys. Rev. Lett. **106**, 183901 (2011).
[9]E. J. Heller, Phys. Rev. Lett. **77**, 4122 (1996).
[10]C. Vanneste and P. Sebbah, Phys. Rev. E **71**, 026612 (2005).
[11]H. Noh, J.-K. Yang, S. F. Liew, M. J. Rooks, G. S. Solomon, and H. Cao, Opt. Lett. **36**, 3560 (2011).
[12]S. F. Liew, J.-K. Yang, H. Noh, C. F. Schreck, E. R. Dufresne, C. S. O'Hern, and H. Cao, Phys. Rev. A **84**, 063818 (2011).
[13]M. Florescu, S. Torquato, and P. Steinhardt, Proc. Natl. Acad. Sci. U.S.A. **106**, 20658 (2009).
[14]Y.-S. No, H.-S. Ee, S.-H. Kwon, S.-K. Kim, M.-K. Seo, J.-H. Kang, Y.-H. Lee, and H.-G. Park, Opt. Express **17**, 1679 (2009).